2007 ASME International Mechanical Engineering Congress and Exposition
November 11-15, 2007, Seattle, Washington, USA

IMECE2007-41494

AN EFFICIENT NUMERICAL SCHEME TO DETERMINE THE PULL-IN PARAMETERS OF AN ELECTROSTATIC MICRO-ACTUATOR WITH CONTACT TYPE NONLINEARITY

Manish M. Joglekar
Research Scholar,
Department of Mechanical Engineering,
Indian Institute of Technology, Bombay.
Mumbai, 400076, India
+91-09892866987 mmjoglekar@iitb.ac.in

Dnyanesh N. Pawaskar
Assistant Professor,
Department of Mechanical Engineering,
Indian Institute of Technology, Bombay.
Mumbai, 400076, India
+91-022-25767548 pawaskar@iitb.ac.in

ABSTRACT

In this article, we present an efficient numerical scheme based on the Rayleigh-Ritz method to determine the pull-in parameters of electrostatically actuated microbeams exploiting contact type nonlinearity. A case of an electrostatically actuated cantilevered microbeam is first analyzed using the Rayleigh-Ritz energy technique. The deflection of the microbeam is approximated by a polynomial trial function. The principle of the stationary potential energy leads to a highly nonlinear algebraic equation, which is solved to determine the deflected shape of the microbeam. A novel voltage iteration algorithm is implemented to determine the critical voltage at which the pull-in occurs. The analysis is then extended to the case of cantilever beam making use of the contact type nonlinearity to exhibit an extended travel range. The present case consists of a compression spring getting engaged at the cantilever tip at the critical point where the pull-in occurs. An increase in both travel range and pull-in voltage is observed with the introduction of the compression spring. A performance index is suggested, which combines the gain in the travel range together with the concomitant increase in the pull-in voltage. This index is used to determine the critical bound for the choice of the stiffness of the newly introduced compression member.

Keywords: - Rayleigh-Ritz method, pull-in instability, pull-in displacement, pull-in voltage, contact type nonlinearity, Pull-in Efficacy Index (PEI)

INTRODUCTION

With the advent in the field of Micro Electro-Mechanical Systems (MEMS), electrostatically actuated micromechanical components have found a prevalent place in many micro systems like micro sensors, microactuators, transducers etc. Compatibility with the microfabrication process, lower power consumption and higher energy densities have made the principle of electrostatic actuation as the most preferred method of actuation in the micro-domain. The electrostatically actuated microbeams have been used in a wide range of applications, which include micro relays [1], capacitive pressure sensors [2], accelerometers [3], micro motors [4] and resonant sensors [5]. Pull-in instability is an inherent phenomenon associated with the use of electrostatic actuation, which is an outcome of the electrostatic-elastic force interaction. In its simplest form, an electrostatic microactuator consists of a movable electrode and a fixed electrode separated by a gap. When a potential difference is applied across these two electrodes, the movable electrode deflects under the influence of the electrostatic force. However, when the displacement of the movable electrode reaches a critical point, it snaps into the fixed electrode. This phenomenon is termed as the pull-in instability [6, 7].

Analysis of the pull-in instability is one of the areas of intense research in the field of electrostatic MEMS. A thorough understanding of this instability would lead to a better design of the actuator system. Although detrimental in many applications, the phenomenon of pull-in instability has been creatively used for material property measurements as well [8].

Several attempts have been made by various researchers to exactly predict the pull-in parameters of the microactuator system. Nathanson et al. [9] modeled the actuator as a lumped spring-mass system and proved that the instability occurs when the movable electrode travels a distance equal to 33% of the initial gap between the two electrodes. The results of their analysis are reviewed in Section 1 of this article. Nemirovsky et al. [6] presented the static analysis of the torsional microactuator and nonlinear parallel plate model with Duffing

type nonlinearity. Elata [10] presented the analysis of voltage and charge controlled parallel plate actuators. Different numerical techniques have been used to solve the electrostatic-elastic coupled field problem. Degani et al. [11] used the displacement iteration algorithm (DIPIE) as against the commonly used Voltage Iteration (VI) algorithm [12]. Kuang et al. [13] used the Differential Quadrature technique to obtain the pull-in parameters. Sadeghian et al [14] made used of finite difference method to predict the behaviour of the microactuator system.

In many commercially used algorithms, separate electrostatic and structural solvers are required to arrive at the solution of the pull-in problem, which makes the solution process time consuming. In this article, we present an efficient numerical scheme based on the Rayleigh-Ritz energy technique to accurately obtain the pull-in parameters. The method is fast, accurate and does not require separate electrostatic and structural solvers.

Travel range extension of electrostatic microactuators is another focus of research in electrostatic MEMS. In some commercial applications like Digital Micromirror Device (DMD) [15], polychromator grating [16]; a higher travel range is required for an adequate operation. To achieve this, pull-in instability needs to be avoided or delayed by implementing some design changes. It is not possible to increase the initial gap between the two electrodes from the fabrication and power requirement perspectives [15, 16]. The travel range extension techniques can be broadly classified into two categories. Active methods include the introduction of an external agency to extend the stable travel range. Current pulse drive [17], folded capacitor design [18] are some of the active methods reported in the open literature. Passive methods include an appropriate change in the microactuator design in order to achieve the extended travel range. Some of the passive methods use leveraged bending [16], prestressed beam [19], biaxial stress [20] and progressive linkage [21].

Recently, we have introduced the concept of piecewise linearity to increase the travel range of the parallel plate model [22]. It has been proved that progressive stiffening of the system at critical points results in a full travel range for parallel plate model. A similar, but structurally different idea has been recently reported by Quio et al. [23]. In this article, we extend the analysis of the piecewise linearity to the case of electrostatically actuated cantilevered microbeam. We make use of the Rayleigh-Ritz energy technique to analyze this coupled field problem involving contact type nonlinearity.

Section 1 reviews the results for the parallel plate model. The Rayleigh-Ritz energy formulation for an electrostatically actuated cantilevered microbeam is presented in Section 2 along with a novel voltage iteration scheme to obtain the critical parameters of the system. In Section 3, the analysis is extended to the case of a cantilever beam with contact type nonlinearity. Results of this analysis are summarized in Section 4. Finally, conclusions are drawn in Section 5.

NOMENCLATURE

A	Area of overlap (parallel plate model)
ε_0	Permittivity of the free space
g_0	Initial gap between the two electrodes forming a microactuator
y^*	Normalized displacement of the microbeam / parallel plate
V^*	Nondimensional form of the applied voltage
α	Mechanical stiffness of the parallel plate model
L	Length of the microcantilever beam
b	Width of the microcantilever beam
h	Thickness of the microcantilever beam
x^*	Normalized length coordinate
E	Young's modulus for the material of the microbeam.
υ	Poisson's ratio
π^*	Normalized total potential energy
$(y^*)_c$	Normalized value of the pull-in displacement for a microcantilever.
K	Stiffness of the compression spring
PEI	Pull-in Efficacy Index

1. PULL-IN INSTABILITY

1.1 Parallel Plate Model of Electrostatic Microactuator

The phenomenon of pull-in instability can be best explained with the help of the parallel plate model shown in Fig.1. The pioneering attempt to analyze this model was reported by Nathanson et al. in 1967 [9].

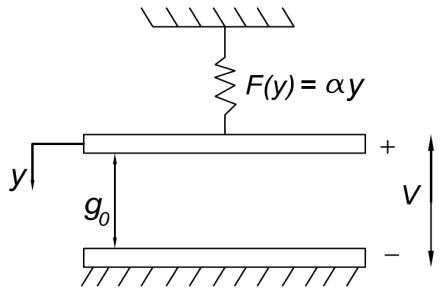

Figure 1 PARALLEL PLATE MODEL OF AN ELECTROSTATIC MICROACTUATOR

This actuator model consists of a top movable electrode capable of offering a linear mechanical restoring force expressed by $F(y) = \alpha y$. When a potential difference V is applied across the actuator plates, the top plate is pulled down under the action of the nonlinearly varying electrostatic force governed by the inverse square law. After the deflection of the movable electrode reaches a critical point, the linear restoring force is no longer able to balance the nonlinear electrostatic force and the movable electrode snaps down into the fixed electrode. This phenomenon is known as the pull-in instability.

The critical displacement of the top electrode at this point is called as the pull-in displacement and the corresponding critical voltage is termed as the pull-in voltage. These two quantities are mathematically expressed as

$$y_{PI} = \frac{g_0}{3} \qquad V_{PI} = \sqrt{\frac{8\alpha g_0^{\,3}}{27 A \varepsilon_0}} \tag{1}$$

A typical voltage-displacement curve for the parallel plate model is shown in Fig.2. The dotted line indicates the unstable equilibrium states for the top movable plate. Figure 2 reveals that the top electrode can be operated stably only up to 1/3rd of the initial gap and thereafter there is no stable equilibrium state for it. This suggests that nearly 66% of the total available range can not be utilized due to the pull-in instability.

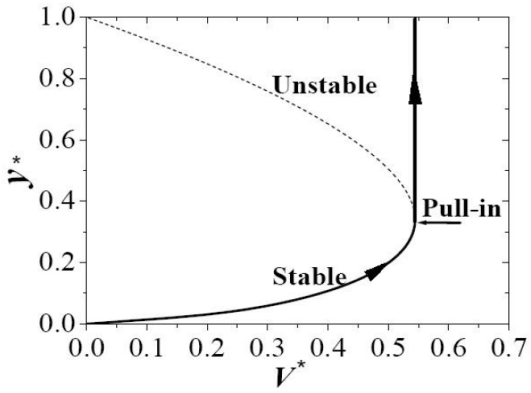

Figure 2 VOLTAGE DISPLACEMENT CHARACTERISTIC OF THE PARALLEL PLATE MODEL

The displacement of the movable plate and the applied voltage can be expressed in a non-dimensional form as

$$x^* = \frac{x}{g_0} \quad , \; V^* = \sqrt{\frac{\varepsilon_0 A V^2}{\alpha g_0^{\,3}}} \tag{2}$$

The numerical values of x^* and V^* at the pull-in are 0.3333 and 0.54433 respectively.

Although the parallel plate model provides a fair insight into the electromechanical behaviour of the actuator, a practical actuator can be closely approximated by a continuous mechanical system such as microbeam, micromembrane or microplate. The primary difference between the parallel plate model and a continuous mechanical system lies in the fact that the stiffness is not constant over the domain in case of the latter. Microcantilever beam is an example of a continuous mechanical system. The stiffness of the beam at the anchored end is very high as compared to the stiffness at the free end. The electrostatic-elastic analysis of such a distributed-stiffness system is more involved than the constant stiffness parallel plate model. In the upcoming section, use of a numerical method based on the Rayleigh-Ritz technique is explained in this context.

2. THE RAYLEIGH-RITZ TECHNIQUE

The governing differential equation of a electrostatically actuated microbeam is nonlinear in nature and is given by

$$EI \frac{d^4 y}{dx^4} = \frac{\varepsilon_0 A V^2}{2(g_0 - y)^2} \tag{3}$$

where *y(x)* is the downward deflection of the microbeam. Equation 3 represents a coupled field system in which the loading on the beam and the deflection of the beam are dependent on each other. Many commercially used algorithms use separate electrostatic and structural solvers to sequentially iterate between the equilibrium solution. However, this makes the solution procedure time consuming. A fast numerical method is generally sought-after to arrive at a fairly accurate solution. We present the formulation and implementation of the Rayleigh-Ritz method to analyze the behavior of the electrostatically actuated cantilevered microbeam.

2.1 Energetics of a Microcantilever Beam

An electrostatically actuated microcantilever beam is schematically shown in Fig.3.

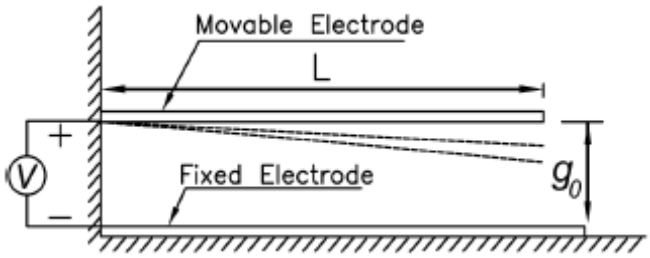

Figure 3 ELECTROSTATICALLY ACTUATED CANTILEVERED MICROBEAM

The principle of operation is similar to that of the parallel plate actuator. The system consists of a movable electrode of length *L*; anchored at its one end and a fixed electrode beneath. The two electrodes are separated by an initial gap equal to g_0. When a potential difference *V* is applied across the two electrodes, the microcantilever beam bends under the action of the electrostatic force. Since the deflection of the microbeam varies along the length, the intensity of the electrostatic force also varies proportionately. The maximum force is experienced by the tip of the cantilever, where the deflection is the maximum.

The deflection of the microbeam is approximated by a known polynomial function $\phi(x)$ and is given by

$$y^*(x^*) = a\phi(x^*) \tag{4}$$

where, the unknown *a* denotes the amplitude of the trial function, which varies with the applied voltage. We choose the

following fourth order polynomial function as a trial function, which satisfies the mechanical boundary conditions of the microcantilever beam.

$$\phi(x^*) = \left(x^*\right)^4 - \left(4x^*\right)^3 + \left(6x^*\right)^2 \tag{5}$$

We assume the microactuator to be a voltage controlled device. The total potential energy of the microbeam in any deflected position can be written as

$$\pi_T = \frac{E'I}{2}\int_0^L (y'')^2 dx - \frac{\varepsilon_0 b V^2}{2}\int_0^L \frac{dx}{(g_0 - y)} \tag{6}$$

where, I is the moment of inertia of the microbeam. E' is the effective Young's modulus for wide beams (b>5h) and is equal to $E/(1\text{-}\upsilon^2)$. In case of narrow beams $E'=E$. Also, $( )'$ denotes the differentiation with respect to x. Equation 6 can be expressed in the normalized form as

$$\pi_T^* = \int_0^1 [(y^*)'']^2 dx^* - (V^*)^2 \int_0^1 \frac{dx^*}{(1 - y^*)} \tag{7}$$

The following normalized parameters are defined

$$x^* = \frac{x}{L} \quad y^* = \frac{y}{g_0} \quad \pi_T^* = \frac{\pi_T L^3}{E'Ig_0^2} \quad V^* = \sqrt{\frac{\varepsilon_0 b L^4 V^2}{2E'Ig_0^3}} \tag{8}$$

The total potential energy of the system is then minimized to find the deflected shape of the system at equilibrium. Making use of Eq. 4 and Eq. 7, we obtain,

$$\frac{d\pi_T^*}{da} = a\int_0^1 (\phi'')^2 dx^* - (V^*)^2 \int_0^1 \frac{\phi dx^*}{(1 - a\phi)^2} = 0 \tag{9}$$

The integral associated with the electrostatic term in Eq. 9 is difficult to carry out analytically and we resort to the three point Gauss rule to integrate the same. Eq. 9 can thus be converted to an algebraic equation of the following form after using the trial function given by Eq. 5.

$$28.8a - \frac{(V^*)^2}{2}\sum_{i=1}^{3} \frac{\phi(\lambda_i) W_i}{[1 - a\phi(\lambda_i)]^2} = 0 \tag{10}$$

where, λ_i's are the transformed Gauss points and W_i's are the weights associated with the Gauss points as given in Table 1.

Table 1 TRANSFORMED GAUSS POINTS AND WEIGHTS

	i=1	i=2	i=3
λ	0.1127	0.5000	0.8873
W	0.5555	0.8888	0.5555

The first term in Eq.10 corresponds to the linear mechanical restoring force while the second term corresponds to the electrostatic force, which is nonlinear in nature.

2.2 The Voltage Iteration Scheme

After simplification, Eq. 10 reduces to a seventh order polynomial equation in terms of a. A total of seven roots can be found out satisfying the polynomial equation, six of which are due to the unstable poles at which the denominator of the electrostatic term becomes zero. So the only root of interest is the one which correspond to the zero of the equation. For each different value of V^*, a unique value of a defines the equilibrium of the system. The critical value of V^* is the one at which the root of interest changes its nature from real to complex indicating the threshold of the stable and unstable equilibrium states of the system.

A voltage iteration algorithm is constructed to extract the critical value of the voltage. The algorithm is schematically shown in Fig. 4.

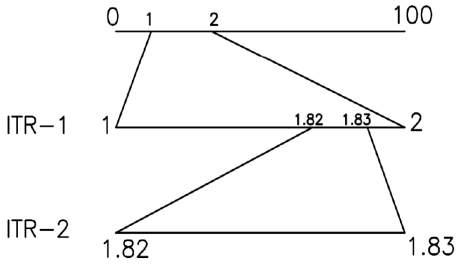

Figure 4 THE VOLTAGE ITERATION SCHEME

It is first assumed that the critical voltage lies between 0 to 100 volts. This range is divided into 100 equal divisions and the nature of the root is checked for each value. The value of the voltage at which the nature is found to be changed, is taken as the upper limit in the next iteration. The immediately preceding voltage value is taken as the lower limit in the next iteration. This process is continued till the required accuracy is obtained. The solution is improved at a rate of two decimal places in every iteration thus assuring the faster rate of the precision.

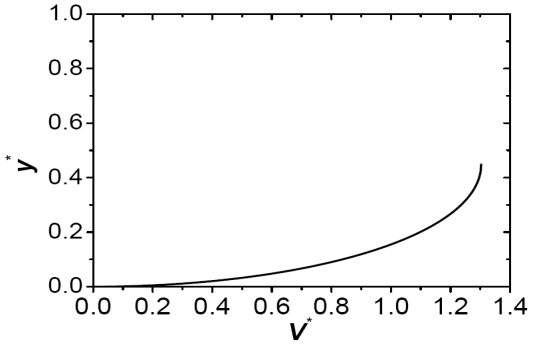

Figure 5 VOLTAGE DISPLACEMENT CHARACTERISTIC FOR A MICROCANTILEVER

For every value of V^*, which is less than the critical value, there exists a root of the polynomial equation which defines the deflected shape of the microbeam in a stable equilibrium. The corresponding voltage displacement characteristics are plotted in Fig.5.

It is observed that the pull-in occurs when the tip of the cantilever beam travels a distance equal to 45% of the initial gap between the two electrodes; as against 33% in case of the parallel plate model.

2.3 Results and Comparison

For an electrostatically actuated microcantilever beam, the normalized pull-in displacement is equal to 0.449 and the normalized voltage at pull-in is equal to 1.303. The exact value of the pull-in voltage can be calculated from the expression in Eq. 8. The obtained results are compared with the previously reported results. The comparison in Table 2 reveals a percentage error around 1.0 in most of the cases, which proves the utility of the numerical technique.

Table 2 COMPARISON OF PULL-IN RESULTS FOR AN ELECTROSTATICALLY ACTUATED MICROCANTILEVER BEAM

Reference	E	υ	L	b	h	g_0	Pull-in Displacement (μm)		Pull-in Voltage (volts)		Percentage Error	
	GPa		μm	μm	μm	μm	Reference	Proposed Method	Reference	Proposed Method	(Pull-in Displacement)	(Pull-in Voltage)
Chowdhury [24]	169	0.32	100	50	3.0	1.0	NA	0.449	39.86	40.30	NA	1.09
2D Model [24]							NA		39.90		NA	0.99
Co-Solve [24]							NA		39.80		NA	1.24
ANSYS							0.451		40.1		0.407	0.49
Chowdhury [24]	169	0.06	150	50	3.0	1.0	NA	0.449	16.83	17.00	NA	1.00
2D Model [24]							NA		16.80		NA	1.18
Co-Solve [24]							NA		16.90		NA	0.59
ANSYS							0.451		16.83		0.407	1.0
Pamidighantam [25]	77	0.33	300	50	1.0	2.5	NA	1.123	2.33	2.3079	NA	0.95
Coventorware [25]							NA		2.25		NA	2.508
ANSYS							1.129		2.29		0.54	0.77

NA: Results not available

3. CANTILEVER BEAM WITH CONTACT TYPE NONLINEARITY

In the previous section, it was shown that the pull-in instability restricts the travel range of the microcantilever beam to nearly 45% of the initial gap between the two electrodes. Different alternatives have been proposed by various researchers to extend the travel range, which have been referred in the introductory note of this article. Our analysis shows that the travel range of the actuator can be effectively increased by stiffening the actuator system at the critical points [22]. Thus, contact type nonlinearity is one of the means to induce the nonlinearity in the mechanical restoring force, thus enabling it to counterbalance the electrostatic force to a greater extent. We have shown that the proposed method is beneficial from both the range increment and from the power perspectives. We extend our analysis to the case of a microcantilever beam exploiting the contact type nonlinearity to exhibit the increased travel range.

3.1 The Energy Formulation for a Microcantilever Beam with an End- Spring.

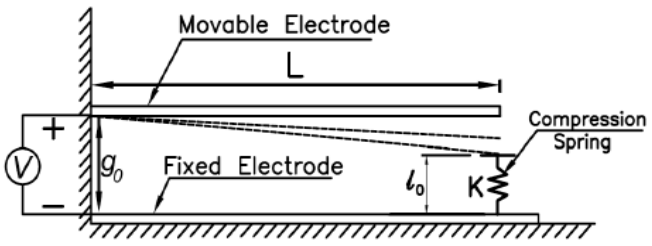

Figure 6 ELECTROSTATICALLY ACTUATED CANTILEVERED MICROBEAM WITH AN END SPRING

The microactuator system under consideration is shown in Fig. 6. With rest of the parameters remaining same, a compression spring of stiffness K is introduced at the tip of the cantilever at the critical point. The uncompressed length of the

spring (l_0) is equal to the unstable range of the microcantilever beam (nearly $0.55g_0$). The spring gets engaged with the tip of the cantilever at the point of instability and thus stiffens the system when it is about to collapse. The analysis remains the same as presented in Section 2 up to the point of engagement of the spring. Thereafter, the newly added compression member alters the energetics of the system.

The deflection of the microbeam beyond the point of engagement of the spring can be approximated by a fourth-order polynomial function $y(x)$

$$y(x) = a_0 + a_1 x + a_2 x^2 + a_3 x^3 + a_4 x^4 \tag{11}$$

By introducing the fixed-end boundary conditions and converting Eq. 11 to a nondimensional form we reduce it to

$$y^* = A_2 (x^*)^2 + A_3 (x^*)^3 + A_4 (x^*)^4 \tag{12}$$

where, y^* and x^* are defined in Eq. 8 and the constants are defined as,

$$A_2 = \frac{a_2 L^2}{g_0} \qquad A_3 = \frac{a_3 L^3}{g_0} \qquad A_4 = \frac{a_4 L^4}{g_0} \tag{13}$$

For the tip displacement more than critical pull-in displacement $(y^*)_c$, the tip boundary conditions are

$$(y^*)''\Big|_{x^*=1} = 0 \tag{14}$$

$$(y^*)'''\Big|_{x^*=1} = \frac{KL^3}{EI}\left(A_2 + A_3 + A_4 - y_c^*\right) \tag{15}$$

Where, K^* is the nondimensional form of the stiffness of the newly added compression member. Normalization is done with respect to the flexural stiffness of the microbeam and is defined as

$$K^* = \frac{KL^3}{EI} \tag{16}$$

Equation 14 and Eq. 15 result in following two simultaneous equations involving 3 unknowns A_2, A_3 and A_4.

$$2A_2 + 6A_3 + 12A_4 = 0 \tag{17}$$

$$6A_3 + 24A_4 = K^*\left(A_2 + A_3 + A_4 - y_c^*\right) \tag{18}$$

Equation 17 and 18 result in the following values of A_2 and A_3, expressed in terms of A_4.

$$A_3 = \alpha_1 A_4 + \beta_1 \qquad \text{and} \qquad A_2 = \alpha_2 A_4 + \beta_2 \tag{19}$$

where the following quantities are defined,

$$\alpha_1 = \frac{-\left(24 + 5K^*\right)}{6 + 2K^*} \qquad \beta_1 = \frac{-K^* y_c^*}{6 + 2K^*} \tag{20}$$

$$\alpha_2 = \frac{\left(36 + 3K^*\right)}{6 + 2K^*} \qquad \beta_2 = \frac{3K^* y_c^*}{6 + 2K^*} \tag{21}$$

Thus, the normalized deflection of the microbeam expressed by Eq. 12 can now be written as

$$y^* = \xi A_4 + \eta \tag{22}$$

where,

$$\xi = \alpha_2 (x^*)^2 + \alpha_1 (x^*)^3 + (x^*)^4 \tag{23}$$

$$\eta = \beta_2 (x^*)^2 + \beta_1 (x^*)^3 \tag{24}$$

The total potential energy of the system can be written as

$$\pi_T^* = \frac{1}{2}\int_0^1 [(y^*)'']^2 dx^* - (V^*)^2 \int_0^1 \frac{dx^*}{(1 - y^*)} + \frac{K^*}{2}\left(y^*\Big|_{x^*=1} - y_c^*\right)^2 \tag{25}$$

The first term in Eq. 25 corresponds to the potential energy due to the bending of the beam, the second term denotes the electrostatic potential energy and the third term arises due to the potential energy stored in the newly engaged compression spring. The principle of stationary potential energy is used to obtain the equilibrium shape for a particular applied voltage. The following equation of equilibrium is obtained for the actuator system from the minimization of the total potential energy

$$\frac{d\pi_T^*}{da} = \int_0^1 (y^*)'' \frac{\partial (y^*)''}{\partial A_4} dx^* - (V^*)^2 \int_0^1 \frac{\left(\partial y^* / \partial A_4\right) dx^*}{(1 - y^*)} + K^*\left(y^*\Big|_{x^*=1} - y_c^*\right)\frac{\partial\left(y^*\Big|_{x^*=1}\right)}{\partial A_4} = 0 \tag{26}$$

Equation 26 is the equilibrium equation of the system and is simplified term by term in the following manner.

Term-I The Beam Bending Term.

From Eq. 22, 23 and 24 we can write,

$$(y^*)'' = \phi A_4 + \theta \tag{27}$$

where,

$$\phi = 2\alpha_2 + 6\alpha_1 x^* + 12(x^*)^2 \tag{28}$$

$$\theta = 2\beta_2 + 6\beta_1 x^* \tag{29}$$

Therefore, the first term in Eq. 26 can be simplified to

$$A_4\int_0^1 \phi^2 dx^* + \int_0^1 \phi\theta dx^* \tag{30}$$

Term-II The Electrostatic Term

From Eq. 22, 23 and 24 we can simplify the second term in Eq. 26 as

$$-(V^*)^2\int_0^1 \frac{\xi dx^*}{(1-(\xi A_4+\eta))^2} \tag{31}$$

which further reduces to

$$-(V^*)^2\int_0^1 \frac{\left(\xi/(1-\eta)^2\right)dx^*}{\left(1-\frac{\xi A_4}{1-\eta}\right)^2} \tag{32}$$

Term-III The Compression Spring Term.

From Eq. 22, 23 and 24 we can write

$$y^*\big|_{x^*=1} = \delta A_4 + \varepsilon \tag{33}$$

where,

$$\delta = \alpha_2 + \alpha_1 + 1 \tag{34}$$

$$\varepsilon = \beta_2 + \beta_1 \tag{35}$$

Therefore the third term in Eq. 26 can be simplified to

$$A_4 K^*\delta^2 + K^*\delta\varepsilon - K^*\delta y_c^* \tag{36}$$

After combining Eq. 30, 32 and 36, we get a simplified form of Eq. 26 as

$$A_4\left(K^*\delta^2 + \int_0^1 \phi^2 dx^*\right) + \left(K^*\delta\varepsilon - K^*\delta y_c^* + \int_0^1 \phi\theta dx^*\right) - (V^*)^2\int_0^1 \frac{\left(\xi/(1-\eta)^2\right)dx^*}{\left(1-\frac{\xi A_4}{1-\eta}\right)^2} = 0 \tag{37}$$

Eq. 37 can be converted to an algebraic equation by definite integration in the first two terms and the numerical integration applied to the electrostatic term.

Eq. 38 can be reduced to a seventh order polynomial equation in A_4, which can be further solved to obtain the value of A_4 for a applied voltage V^*. This value of A_4 determines the equilibrium shape of the microbeam which can be determined from Eq. 22.

$$A_4\left(\frac{144}{5} + 36\alpha_1 + 12\alpha_1^2 + 16\alpha_2 + 12\alpha_1\alpha_2 + 4\alpha_2^2 + K^*\delta^2\right) + K^*\delta\varepsilon - K^* y_c^*\delta + 18\beta_1 + 12\alpha_1\beta_1 + 6\alpha_2\beta_1 + 8\beta_2 + 6\alpha_1\beta_2 + 4\alpha_2\beta_2 - \frac{(V^*)^2}{2}\sum_{i=1}^{3}\frac{\left(\xi(\lambda_i)/(1-\eta(\lambda_i))^2\right)W_i}{\left(1-\frac{\xi(\lambda_i)A_4}{1-\eta(\lambda_i)}\right)^2} = 0 \tag{38}$$

Some important results pertaining to the pull-in instability of this system are discussed in the next section.

4. RESULTS AND DISCUSSIONS

The pull-in behaviour of the microcantilever system in the absence of the compression spring has been discussed in Section 2. The behaviour of the system with a compression spring getting engaged at the critical position largely depends on the stiffness of the compression spring in comparison with the flexural stiffness of the microcantilever. Both these terms have been combined to form a nondimensional stiffness parameter defined in Eq. 16. As the value of K^* changes, the static behavior of the system also changes, which in turn affects the pull-in parameters.

With an increasing value of K^*, the deflection profile (elastica) of the microcantilever beam changes after the engagement of the compression spring. This is illustrated in Fig.7, in which the deflection profile of the cantilever beam at pull-in is plotted for different values of K^*.

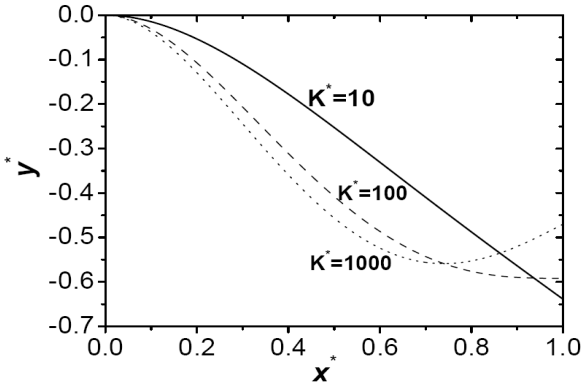

Figure 7 ELASTICA OF THE MICROBEAM AT PULL-IN FOR DIFFERENT VALUES OF K^*

For sufficiently smaller values of K^* (below 100), the tip of the cantilever experiences the maximum deflection. However, if the stiffness parameter is more than the stated value, the spring is so stiff that, under the influence of the electrostatic force some other section of the beam, which is nearer to the tip starts deforming downwards. Since the electrostatic force follows the inverse square law, the same acting on this deformed section keeps on increasing with increasing voltage.

Ultimately, the section experiences the pull-in instability. Thus the beam-section which is snapped into the bottom electrode is not the tip anymore for higher values of K^* which can be seen in Fig. 7 for K^*=1000.

It has been shown that the microcantilever beam without a compression spring, experiences the instability after traveling nearly 45% of the initial gap. The curve for K^*=10 in Fig. 7 shows that, at the time of pull-in, the tip of the cantilever has traveled more than 45% of the initial gap, thus indicating the increament in the range of the actuator.

In this connection, we study the voltage-displacement characteristics for the system for different representative values of K^*. This helps in understanding the variation in the value of the pull-in displacement for different values of the spring stiffness. However, it should be noted that the tip displacement is not the maximum in every case as indicated in Fig.7. Hence, we plot the voltage-minimum gap characteristics for the system in Fig.8.

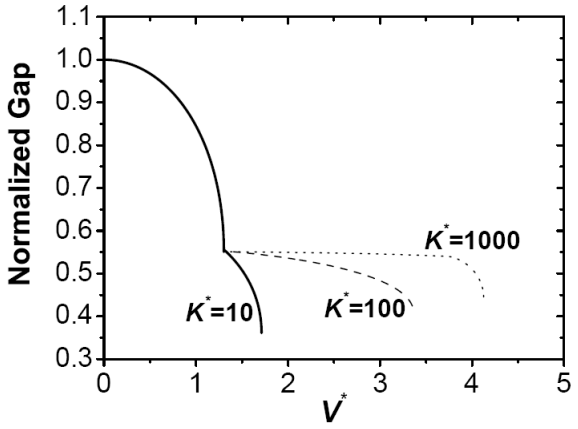

Figure 8 VOLTAGE-MINIMUM GAP CHARACTERISTICS FOR DIFFERENT VALUES OF K^*

Figure 8 depicts the variation of the maximum displacement in the beam with respect to the increasing voltage. Initially the microbeam is in the undeformed position and the normalized gap value is equal to 1.0. When the voltage is increased, the beam deflects downwards and the gap decreases. It should be noted that till the time the beam reaches the first critical position there is no role of the compression spring and the decreasing gap represents the increasing tip deflection. After the engagement of the compression spring, the behaviour is dependent on the nondimensional stiffness parameter. For K^*=10, the tip deflection is the maximum deflection in the beam, and the pull-in occurs when the tip is displaced by 63.88% of the initial gap (which also refers to a normalized gap of 0.36 in Fig.8). The normalized value of the pull-in voltage is equal to 1.711 at this point. Thus it can be said that there is 42.22% increase in the normalized pull-in displacement and 31.39% increase in normalized the pull-in voltage, when compared with the microbeam behaviour without the compression spring.

As the value of K^* is increased further, the characteristics in Fig. 8 changes significantly. For K^*=100, the normalized pull-in displacement is decreased (0.591), however, there is a significant increase in the normalized pull-in voltage (3.364). An interesting trend is observed for K^*=1000. Tip displacement is the maximum displacement up to the first critical point. Due to a very high stiffness, the tip remains in an almost held position even if the voltage is increased. There exists a beam section apart from the tip, which starts deforming towards the fixed electrode. Till the time, its displacement becomes equal to the held displacement of the tip; the maximum displacement of the system remains same as the tip displacement. This can be seen in form of a constant gap line in Fig.8. Soon after, the displacement of deforming section exceeds the tip displacement and experiences the pull-in instability, which is indicated by an end curve for K^*=1000. The normalized pull-in displacement and the normalized pull-in voltage for this case are 0.558 and 4.127 respectively.

It is clear from the previous discussion that, the normalized pull-in displacement and the normalized pull-in voltage are altered by the choice of K^*. Also, it is evident that as the value of K^* is changed, the tip displacement and the maximum tip displacement do not remain the same. This is quantitatively plotted in Fig.9.

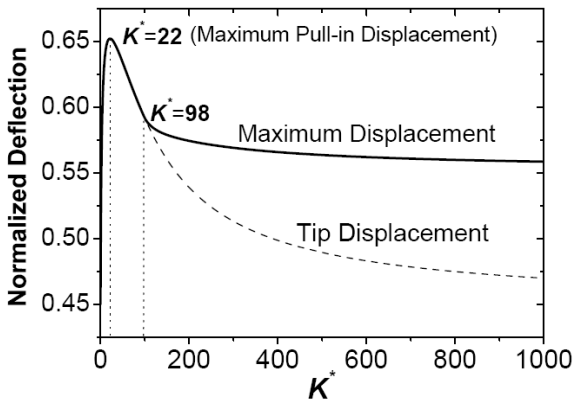

Figure 9 VARIATION OF THE NORMALIZED DISPLACEMENT WITH K^*

For very small values of K^* (less than 0.1), the normalized pull-in displacement is nearly same as that of a microbeam without a compression spring (approximately 0.449). The maximum pull-in displacement of the system is equal to 0.652 and occurs at a value of K^*=22. After that, the pull-in displacement is decreased due to the increased stiffness of the compression spring. Another significant point is reached when K^*=98. Up to this point the tip displacement is the maximum displacement, but after that the maximum displacement takes place at some other section of the beam. For a very high value of K^*, (K^*=100000), the normalized tip displacement converges to 0.449. This indicates the rigid support getting engaged at the tip when the pull-in is about to occur. The maximum normalized pull-in displacement in this case is equal to 0.553, which occurs at a normalized length of 0.727 from the fixed end.

It is evident from Fig.8 that, the normalized pull-in voltage increases with the increase in the value of K^*. This is true because the stiffness of the system is increased and more electrostatic force is required to deform the system. The variation of the normalized pull-in voltage with K^* is shown in Fig.10.

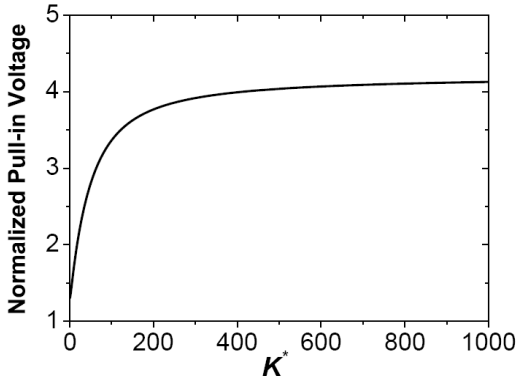

Figure 10 VARIATION OF THE NORMALIZED PULL-IN VOLTAGE WITH K^*

Figure 10 shows a converging nature of the normalized pull-in voltage with the increasing value of K^*. For a very high value of K^* (K^*=100000), the pull-in voltage converges to a value of 4.216, showing a percentage increase of 223.57 over the same value for the microcantilever without compression spring.

With the change in the stiffness of the compression spring, both, pull-in displacement as well as pull-in voltage change. Pull-in displacement shows an increasing nature first and decreases later on (Fig. 9), while the pull-in voltage shows a converging trend (Fig. 10). Generally, it is required to achieve higher travel range without increasing the actuation voltage by a significant amount. We combine both aforementioned variations in a single nondimensional parameter termed as the Pull-in Efficacy Index (PEI) which is defined as

$$\textbf{PEI} = (\%\ \text{change in PuD}) - (\%\ \text{change in PuV}) \qquad (39)$$

where PuD and PuV denote the normalized pull-in displacement and the normalized pull-in voltage respectively. The base values to calculate the percentage changes are taken as those of the microcantilever beam without compression spring. The value of the PEI, should necessarily be positive in order to attain higher travel range at a lower cost of the actuation voltage increase. The value of the PEI ceases to be positive after K^*=14. We plot the variation of the PEI with respect to K^* up to this range in Fig 11.

Figure 11 shows a distinct peak in the variation of the PEI at K^*=3.92. The value of the PEI at this point is equal to 21.565. The corresponding values of the normalized pull-in displacement and the normalized pull-in voltages are 0.593 and 1.439 respectively.

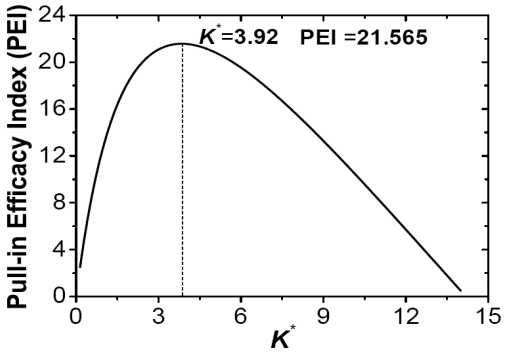

Figure 11 VARIATION OF PULL-IN EFFICACY INDEX WITH K^*

It can be thus concluded that the optimum stiffness of the spring is approximately 4 times the flexural stiffness of the microbeam, which yields maximum pull-in displacement with minimal increase in the pull-in voltage.

5. CONCLUSION

The present study provides an insight into the pull-in behaviour of the microcantilever beam, with and without the compression spring getting engaged at the critical position. The Rayleigh-Ritz energy method has been effectively used to analyze the electrostatic-elastic problem under consideration. The numerical method does not require separate electromechanical solvers and is fast as well as accurate as compared to the commercially used algorithms. The analysis of a microcantilever by using the proposed numerical technique shows that, the normalized pull-in displacement is equal to 0.449 and the normalized pull-in voltage is equal to 1.303. The exact operational values of the pull-in displacement and the pull-in voltage can be obtained from the normalization definitions in Eq.8.

The compression spring getting engaged at the critical point of the cantilever beam changes the energetics of the system and the system behaviour depends on the stiffness of the compression spring. A nondimensional stiffness parameter K^* is defined (Eq. 16) to quantitatively predict the performance of the system.

Up to the value of K^*=22, an increase in the normalized pull-in displacement is observed, which decreases thereafter, the maximum being 0.652. For very high values of K^*, the spring acts as a rigid support and the maximum pull-in displacement converges to 0.553, but occurs at a normalized length of 0.727 from the fixed support.

Up to the value of K^*=98, the pull-in takes place at the tip, which experiences the maximum deflection. Beyond this value the maximum deflection does not occur at the tip but at some other section of the beam.

Normalized pull-in voltage shows an increasing trend with the increase in the K^* value, which slowly converges to a value of 4.216 for a very high value of K^*.

The changes in the normalized pull-in displacement and the normalized pull-in voltage are combined together in form a nondimensional parameter termed as the Pull-in Efficacy Index (PEI) (Eq. 39). This parameter is used to find the optimum value of K^*, for which maximum gain in the pull-in displacement is obtained with a minimum increase in the pull-in voltage. The optimum value is equal to K^*=3.92 and the corresponding values for the normalized pull-in displacement and the normalized pull-in voltage are 0.593 and 1.439 respectively.

The analysis is useful in designing the system having an increased travel range by using the piecewise linear technique to make the mechanical restoring force nonlinear. A secondary cantilever made up of the insulating material can be thought as a practical implementation of the compression spring. The choice of design parameters for this secondary cantilever can be made from the critical stiffness parameter values obtained in the analysis.

6. ACKNOWLEDGEMENTS

The authors greatly acknowledge the support from Suman Mashruwala Microengineering Laboratory (SMAμL), IIT Bombay; a facility created with the generous donation from Mr. Raj Mashruwala. Authors would also like to thank Prof. P.S. Gandhi, IIT Bombay, Dr. K.Y. Hardikar, Novellus Systems and Mr. Samarth Raut, Applied Materials for many useful discussions.

7. REFERENCES

[1] Schiele, I., Huber, J., Hillerich, B., and Kozlowski, F., 1998, “Surface Micromachined Electrostatic Microrelay”, Sensors and Actuators A., 66(1-3), pp. 345-354.

[2] McIntosh, R.B., Mauger, P.E., and Patterson, S.R., 2006, “Capacitive transducers with curved electrodes,” IEEE Sensors Journal, 6(1), pp.125-138.

[3] Gerlach-Meyer, U. E., 1991, “Micromachined Capacitive Accelerometer,” Sensors and Actuators A, 27 (1-3), pp. 565-569.

[4] Baginsky, I.L., and Kostsov, E.G., 2003, “High energy capacitance electrostatic micromotors,” Journal of Micromechanics and Microengineering, 13(5), pp.190-200.

[5] Abdel Rehman, E.M., Nayfeh, A.H., and Younis M.I., 2003, “Dynamics of an Electrically Actuated Resonant Microsensor,” Proceedings of the International Conference on MEMS, NANO and Smart Systems ICMENS’03, IEEE, Canada, pp. 188-196.

[6] Nemirovsky, Y., and Bochobza-Degani, O., 2001, “A Methodology and Model for the Pull-in Parameters of Electrostatic Actuators,” Journal of Microelectromechanical Systems, 10(4), pp.601-615.

[7] Yang, F., 2002, “Electromechanical instability of microscale structures,” Journal of Applied Physics, 92(5), pp. 2789-2794.

[8] Osterberg, P.M., and Senturia, S.D., 1997, “M-TEST: A Test Chip for MEMS Material Property Measurement Using Electrostatically Actuated Test Structures,” Journal of Microelectromechanical Systems, 6(2), pp.107-118.

[9] Nathanson, H., Newell, W., Wickstrom, R., and Davis, J.R., 1967, “The resonant gate transistor,” IEEE Transactions on Electronics Devices, 14(3), pp.114-133.

[10] Elata, D., “On Static and Dynamic Response of Electrostatic Actuators”, 2005, Bulletin of the Polish Academy of Sciences, Technical Sciences, 53(4), pp. 373-384.

[11] Degani, O., Elata D., and Nemirovsky Y., 2002, “An Efficient DIPIE Algorithm for CAD of Electrostatically Actuated MEMS devices,” Journal of Microelectromechanical Systems 11(5), pp. 612–620.

[12] Fischer M., Giousouf M., Schaepperle J., Eichner D., Weinmann M., Von Munch W., and Assmus F., 1998, “Electrostatically Deflectable Polysilicon Micromirrors—Dynamic Behavior and Comparison with Results from FEM Modeling with ANSYS,” Sensors and Actuators A., 67, pp. 89–95,

[13] Kuang J., and Chen C., 2005, “The Nonlinear Electrostatic Behavior for Shaped Electrode Actuators,” International Journal of Mechanical Sciences 47, pp. 1172–1190.

[14] Sadeghian H., and Rezazadeh G., 2006 “The influence of stress gradient on the pull-in phenomena of microelectromechanical switches,” Journal of Physics, 34, pp. 1117–1122.

[15] Bifano, T.G., Perreault, J., Mali, R.K., Horenstein, M.N., 1999, “Microelectromechanical Deformable Mirrors,” IEEE Journal of Selected Topics in Quantum Electronics, 5(1), pp.83-89.

[16] Hung, E.S., and Senturia, S.D., 1999, “Extending the Travel Range of Analog-Tuned Electrostatic Actuators,” Journal of Microelectromechanical Systems, 8(4), pp.497-505.

[17] Castaner, L., Pons, J., Nadal-Guardia, R., and Rodriguez, A., 2001, “Analysis of the extended operation range of electrostatic actuators by current-pulse drive,” Sensors and Actuators A, 90(3), pp. 181-190.

[18] Chan, E.K., and Dutton, R.W., 2000, “Electrostatic Micromechanical Actuator with Extended Range of Travel,” Journal of Microelectromechanical Systems, 9(3), pp. 321-328.

[19] Chiou, J.C., and Lin, Y.J., 2005, “A novel large displacement electrostatic actuator: pre-stress comb-drive actuator,” Journal of Micromechanics and Microengineering, 15(9), pp. 1641-1648.

[20] Gray, G.D., Morgan, M.J., and Kohl, P.A., “Electrostatic Actuators with Expended Tuning Range Due to Biaxial Intrinsic Stress Gradients,” Journal of Microelectromechanical Systems, 13(1), pp.51-62.

[21] Bronson, J.R., Wiens, G.J., and Allen, J.J., 2005, “Modeling and Alleviating Instability in a MEMS Vertical Comb Drive using a Progressive Linkage,” Proceedings of IDETC/CIE-2005, ASME, California, DETC2005-84217, 24-28.

[22] Joglekar M., and Pawaskar D., 2007, "Travel Range Extension of an Electrostatic Microactuator: Nonlinear Parallel Plate Models", Proceedings of the International Conference on Emerging Mechanical Technology: Macro to Nano EMTM2N 2007, BITS, Pilani, India, pp. 171-178.

[23] Quio, D., Yuan, W. and Li., X., 2006, “A two-beam method for extending the working range of electrostatic parallel-plate micro-actuators”, Journal of Electrostatics, doi:10.1016/j.elstat.2006.09.001

[24] Chowdhury, S., Ahmadi, M., and Miller W., 2005, “A Closed Form Model for the Pull-in Voltage of Electrostatically Actuated Cantilever Beams, Journal of Micromechanics Microengineering, 15, pp. 756-763.

[25] Pamidighantam, S., Pures, R., Baert, K., Tilmans, A., 2002, “Pull-in voltage analysis of electrostatically actuated beam structures with fixed-fixed and fixed-free end conditions”, Journal of Micromechanics Microengineering, 12, pp.458-464.

